CHEMISTRY OF MATERIALS

pubs.acs.org/cm

Article

Intrinsic Pore Architecture of a Two-Dimensional MOF: A Blueprint for Overcoming the Permeability-Selectivity Trade-Off in Desalination

Dong Fan, Ke Zheng, Supriyo Naskar, and Guillaume Maurin*

Cite This: *Chem. Mater.* 2025, 37, 8627−8635

Read Online

ACCESS | Metrics & More | Article Recommendations | Supporting Information

ABSTRACT: Water scarcity remains one of the most pressing global challenges, driving the urgent need for next-generation desalination technologies that can overcome the long-standing trade-off between water permeability and ion selectivity. Here, we introduce a molecular design blueprint based on a two-dimensional metal−organic framework (2D-MOF) monolayer, $NiF_2(pyz)_2$, featuring intrinsically aligned ∼4 Å pores and high structural regularity. Using systematic all-atom molecular dynamics simulations, we demonstrate that this monolayer achieves ultrahigh water permeability while maintaining 100% Na^+/Cl^- rejection across a wide range of applied pressures. We attribute this exceptional performance to a synergistic combination of low interfacial water density, reduced free energy barriers for water transport, and a high pore area-to-surface area ratio, captured by a proposed dimensionless descriptor. Compared to conventional 2D membranes with artificial nanopores, which often suffer from fabrication complexity, pore size variability, and mechanical fragility, the $NiF_2(pyz)_2$ monolayer offers a robust alternative with precisely defined nanochannels combined with mechanical and hydrothermal stability. This work pushes the boundaries of the structure−function paradigm in membrane science by establishing that atomically engineered intrinsic porosity, rather than postfabricated artificial channels, is the key to achieving fast and selective water transport. Our findings lay the groundwork for the rational design of high-efficiency desalination membranes and suggest possible approaches for using MOFs in sustainable water purification technologies.

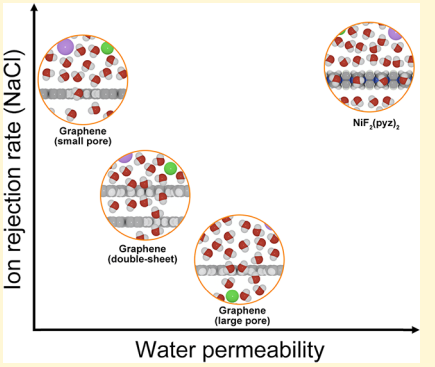

INTRODUCTION

As populations grow and industrialization expands, the demand for fresh water is intensifying, making global water scarcity one of the most pressing challenges of our time.[1−3] To address this challenge, researchers are diligently exploring a diverse range of cutting-edge technologies and solutions to effectively purify, decontaminate, desalinate, and optimize the quality of water. Desalination technologies have garnered significant interest as promising solutions to water scarcity, with multistage flash distillation (MSF), multieffect distillation (MED), and reverse osmosis (RO) representing the leading approaches. RO membranes have experienced swift market traction owing to their exceptional efficiency in separating water molecules from dissolved salts and impurities.[4] This high-pressure membrane technology primarily leverages a semipermeable polymer or a porous material membrane to selectively retain salts and low molecular weight solutes while allowing water molecules to permeate through.[5] The separation mechanism is fundamentally linked to the pore size of the porous material:[6,7] For pores in the angstrom range (∼4 Å), transport is dominated by molecular sieving: hydrated ions are excluded due to their larger size, while water molecules permeate rapidly. As pore size increases, transport becomes more continuous, enhancing permeability but often compromising ion rejection, leading to the well-known permeability-selectivity trade-off.[8] Despite its widespread deployment, reverse osmosis (RO) still faces key technical bottlenecks, including limited conversion efficiency, membrane fouling, and high energy demands for pressurizing feedwater. Advancing next-generation membrane materials is therefore crucial to enhance both performance and sustainability in water purification. A promising direction lies in the rational design of tailored pore architectures within conventional materials and in the exploration of novel membranes derived from intrinsically porous nanomaterials.[9,10]

Metal−organic frameworks (MOFs) have received considerable attention because of their potential applications in gas adsorption/separation,[8] catalysis,[9,10] and sensors.[11] Remarkably, a rational selection of the organic linkers and the metal nodes enables tailoring the pore size/shape/topology and the functionality of the MOFs targeted for a given applica-

Received: June 16, 2025
Revised: October 18, 2025
Accepted: October 20, 2025
Published: October 29, 2025

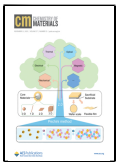

https://doi.org/10.1021/acs.chemmater.5c01510
Chem. Mater. 2025, 37, 8627−8635

tion.[8,12−14] Despite that MOF-based membranes have shown excellent separation performance for diverse gas mixtures,[15−17] their application in desalination is still scarce, primarily due to the limited hydrothermal stability of certain MOFs, which restricts their use in aqueous environments. Nonetheless, several MOFs have already demonstrated potential as candidates for water desalination, highlighting this area as an emerging and promising field of research.[18,19] The UiO-66(Zr)-based membrane was first reported with a moderate water permeability (approximately 0.14 L m^{-2} h^{-1} bar^{-1}) and 45.7−99.8% ion rejection rate depending on the nature of the ions.[18] Owing to the large chemical and structural versatility of this family of materials, a few other MOFs have been considered for water desalination including UIO-66-NH_2, ZIF-8, Al-TCPP, and MOF-303, among others.[20−23] Therefore, MOF-based membranes still face challenges related to low water permeability and limited ion rejection efficiency.

The optimal active material for desalination membranes should feature pores small enough to reject ions, yet sufficiently large to enable rapid water transport.[24−26] Building on this requirement, we propose that MOF structures with 1D channels represent a promising and viable class of materials for water desalination. We have recently designed a mechanically and water stable 2D-MOF, NiF_2(pyrazine)$_2$ (labeled as $NiF_2(pyz)_2$).[27] Its intrinsic nanochannels, with a pore size of approximately 4 Å, exceed the kinetic diameter of water (2.64 Å), enabling its migration toward the pores[28] while it is expected to prevent the formation of water clusters, known to diffuse more slowly than isolated molecules.[29] Therefore, the $NiF_2(pyz)_2$ monolayer is anticipated to exhibit high water permeability, leading to fast water transport across the membrane (*cf.* Scheme 1).

Herein, we harness advanced molecular dynamics (MD) simulations to explore the water transport and ion rejection kinetics of the 2D-$NiF_2(pyz)_2$ MOF membrane, benchmarked against the [001]-oriented membrane of the structurally analogous 3D **ALFFIVE**-1-Ni MOF that has been previously reported with exceptional gas separation performance thanks to its ultrasmall porosity.[30] This comparative investigation unravels the fundamental molecular-level mechanisms driving the exceptional desalination performance of this 2D MOF, which is characterized by ultrahigh water flux and selective ion exclusion. Our findings reveal that the 2D-$NiF_2(pyz)_2$ membrane achieves outstanding water permeability alongside 100% Na^+/Cl^- rejection, surpassing the performance of earlier 2D materials incorporating structurally inhomogeneous artificial channels.

Conventional 2D desalination membranes often rely on artificially created nanopores that typically exhibit structural inhomogeneity. This inherent irregularity fundamentally limits their performance, manifesting as a persistent trade-off between water permeability and ion rejection. Defying the conventional design paradigm that prioritizes enlarged pore sizes to enhance water flux, we show that engineering MOF membranes with intrinsically uniform ultrasmall nanochannels (~14.9 $Å^2$) can deliver both very high permeability and complete ion rejection. The 2D-$NiF_2(pyz)_2$ membrane exhibits a water permeability nearly three times higher than state-of-the-art MoS_2-based membranes, while maintaining 100% Na^+/Cl^- exclusion, thereby establishing a potential materials design strategy that reconciles the long-standing trade-off between permeability and selectivity in desalination.

Scheme 1. Illustrations of Water Transport through the Distinct Membranes[a]

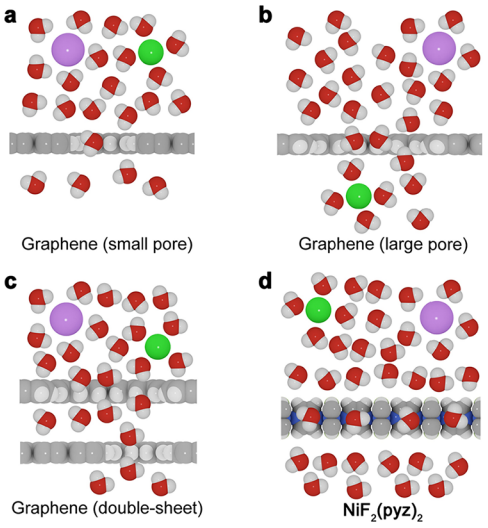

[a](a) The nanoporous graphene model with a small pore size is expected to exhibit a high ion rejection rate but low permeability. (b) The nanoporous graphene model with a large pore size is anticipated to lead to enhanced water permeability but at the expense of a decrease of the rejection rate. (c) For the double-layer nanoporous graphene model, the ion rejection rate is expected to be improved, but water permeability is still limited compared with the nanoporous graphene model with large pore size. (d) The MOF monolayer membrane with intrinsic small pore size is anticipated to show high water permeability and 100% ion rejection rate

METHODS

All-atom structures of the membranes, **AlFFIVE**-1-Ni, $NiF_2(pyz)_2$, **Gr_1**, and **Gr_2**, were built on the basis of the DFT results. Molecular dynamics (MD) simulations were performed using the LAMMPS code.[31] The simulation boxes with graphene piston, saline water, membranes, and water molecules were visualized by the Visual Molecular Dynamics (VMD, 1.9.3 version).[32] The saline water box contains Na^+/Cl^- ions with a molarity of ~0.63 M, similar to that in natural seawater. More details about the model used in this work are provided in the Supporting Information. The TIP4*P*/2005 water model was used,[33] and the SHAKE algorithm[34] with 10^{-5} accuracy tolerance was employed to maintain the rigidity of the water molecules. Other water models[35,36] were considered leading to similar results as summarized in Supplementary Figure S1. For nonbonded interactions, the Lorentz−Berthelot rule was used to obtain the Lennard-Jones (LJ) parameters.[37] The LJ parameters are listed in the supplementary tables. The LJ cutoff distance was set as 12 Å. The long-range electrostatic interactions were treated by the Ewald sum method.[38] Periodic boundary conditions were applied in all three directions. For each individual simulation, the energy of the boxes was first minimized for 1.0×10^4 steps. Next, the boxes were equilibrated under the *NPT* ensemble with a temperature of 300 K and a pressure of 1 bar for 2 ns simulations. Membranes were fixed during the equilibrium process, and finally, the *NPT* simulations enabled water to reach its equilibrium density (~1 g cm^{-3}).

After *NPT* equilibration, the *NVT* ensemble was performed using the Nosé−Hoover thermostat.[39,40] The MD production run was achieved with a time constant of 0.1 ps for 10 ns (more than 20 ns for the **AlFFIVE**-1-Ni membrane). During the production run, the rigid piston applied a constant pressure ranging from 25 to 350 MPa on saline water to simulate water filtration through membranes. The 2D membranes were held fixed during the production run, while the **AlFFIVE**-1-Ni membrane was simulated by the fully flexible force field with the universal force field (UFF).[41] Consistent with our previous research,[17] partial charges of the **AlFFIVE**-1-Ni slab and 2D

https://doi.org/10.1021/acs.chemmater.5c01510
Chem. Mater. 2025, 37, 8627−8635

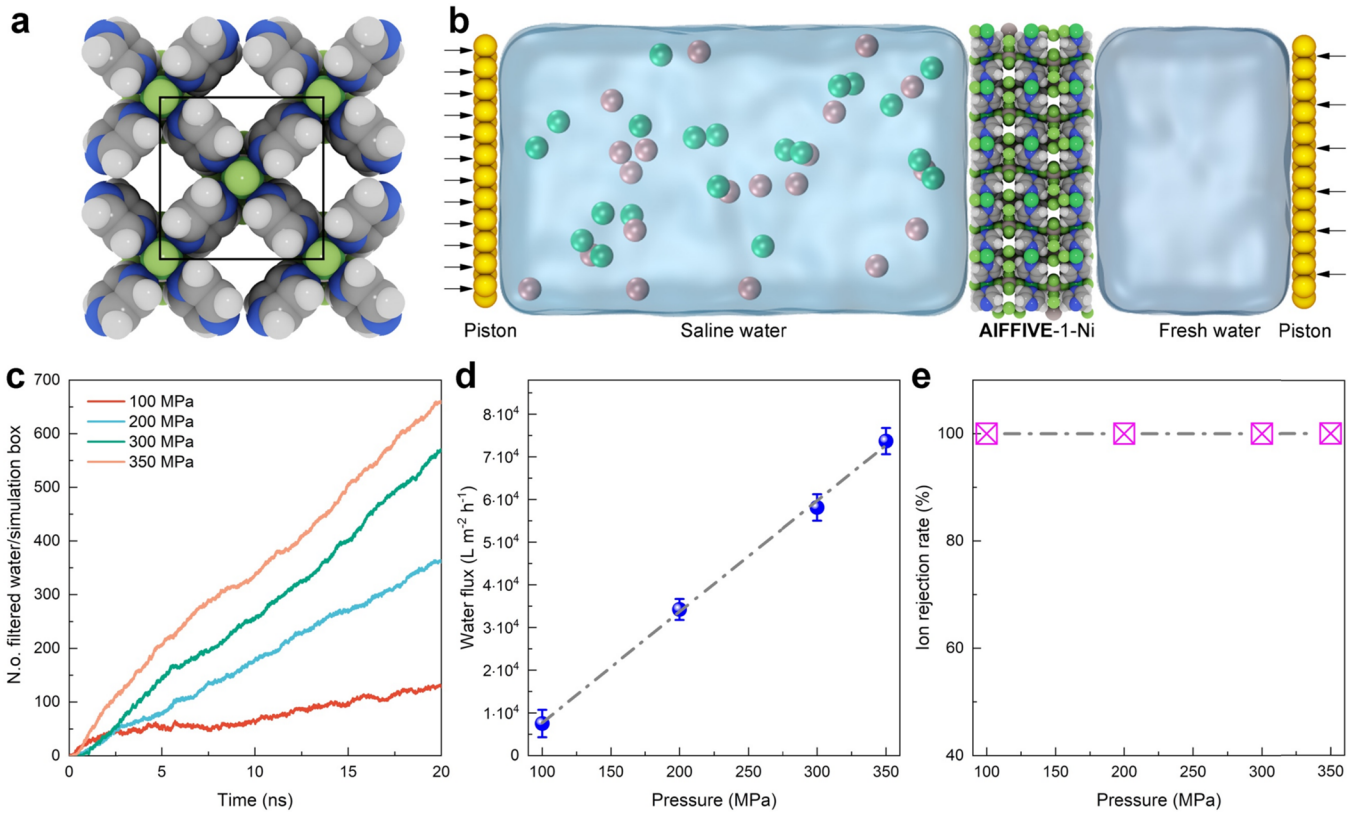

Figure 1. Water transport/salt rejection through the [001]-oriented **AlFFIVE**-1-Ni MOF membrane. (a) Top view of the bulk **AlFFIVE**-1-Ni crystal structure along the 1D channel direction ([001]). Color scheme: C, gray; H, white; Ni, cyan; F, green; N, blue; Al, purple. (b) Schematic of the membrane simulation box consisting of a piston, saline water with Na^+ and Cl^- ions, [001]-oriented **AlFFIVE**-1-Ni MOF membrane, and freshwater section. (c) Number of water molecules passing through the **AlFFIVE**-1-Ni MOF as a function of the MD simulations at distinct applied pressures of 100, 200, 300, and 350 MPa. (d) Water flux as a function of the applied pressure for **AlFFIVE**-1-Ni MOF. The error bars were extracted from three independent MD runs. (e) Ion rejection rate (Na^+/Cl^-) of the **AlFFIVE**-1-Ni MOF membrane with respect to the external pressure.

$NiF_2(pyz)_2$ membrane were computed using the DDEC06 method.[42] The Ni atoms of the **AlFFIVE**-1-Ni membrane were fixed to hold the membrane during the nonequilibrium simulations (Movie S1 and Movie S2). Trajectories under different pressures were collected every 5 ps to obtain the results. Further details on the models, simulation details, and force field parameters are provided in the Supporting Information.

RESULTS AND DISCUSSION

Water Transport/Salt Rejection through the [001]-Oriented AlFFIVE-1-Ni Membrane. To establish a theoretical foundation, we examined the performance of the orientated **AlFFIVE**-1-Ni MOF, which features ultrasmall pore channels, as shown in Figure 1a. The simulation box, depicted in Figure 1b, consists of saline water (Na^+ and Cl^- with a model concentration: molarity ~0.63 M) on the feed side and fresh water on the permeate side separated by a **AlFFIVE**-1-Ni membrane oriented along the channel ([001] direction). Water molecules on both sides of the **AlFFIVE**-1-Ni membrane can be exchanged consistently, and when a transmembrane pressure gradient is applied under nonequilibrium conditions, fresh water flows from the feed side to the permeate side through the **AlFFIVE**-1-Ni membrane (*cf.* Supplementary Movie S1). Figure 1c shows the plot of the number of filtered water molecules passing through the **AlFFIVE**-1-Ni membrane as a function of the MD simulation time under different applied pressures (tests for different water models can be found in Supplementary Figure S1, Tables S1−S4). All curves show a linear trend with MD simulation time, indicating that a steady water flow driven by the applied feed pressure was achieved in all of the MD simulations. Figure 1d reports the calculated water flux by fitting the data reported in Figure 1c and its dependence with respect to the applied feed pressures. Within the simulated pressure range, the water flux exhibits a linear dependence on the applied pressure, in agreement with the theoretical prediction of continuous flow. Importantly, the **AlFFIVE**-1-Ni membrane shows an excellent water permeability (14.32 L m^{-2} h^{-1} bar^{-1}) 2 orders of magnitude higher than the performance previously reported for other MOFs including UiO-66(Zr) (0.14 L m^{-2} h^{-1} bar^{-1}) and MOF-303 (0.74 L m^{-2} h^{-1} bar^{-1}).[18,21,43] The cage-like porosity of UiO-66(Zr) tends to reduce the overall water permeability. In contrast, the channel-like **AlFFIVE**-1-Ni makes potential energy barriers for water to cross the membrane much smaller and increases the overall water permeability. The salt rejection rate of the **AlFFIVE**-1-Ni membrane was further calculated by analyzing the MD trajectories of sodium ions and chloride ions under the different applied pressures as shown in Figure 1e. The salt rejection rate was found to be 100% under all of the applied feed pressures. As the hydrated radii of Na^+ (~7.16 Å)[28] and Cl^- (~6.64 Å)[28] are substantially larger than the pore size of **AlFFIVE**-1-Ni (~4.0 Å), the associated free energy barrier for their translocation across the membrane is expected to be high.

https://doi.org/10.1021/acs.chemmater.5c01510
Chem. Mater. 2025, 37, 8627−8635

Remarkably, the Na^+/Cl^- rejection efficiency remains at 100% even under applied pressures as high as 350 MPa, underscoring the theoretical suitability of the **AlFFIVE**-1-Ni pore size and morphology for advanced water desalination membrane design.

Design of an Effective Monolayer $NiF_2(pyz)_2$ Membrane for Water Desalination. Although the **AlFFIVE**-1-Ni membrane is predicted to outperform conventional MOFs in terms of ion rejection and water permeability, the stabilization of high-aspect-ratio [001] nanosheets in solution is difficult to achieve. Moreover, its inherently small pore size (~4 Å) necessitates the use of ultrathin nanosheets to enable efficient seawater desalination. A monolayer structure constitutes the thinnest possible form of an ultrathin nanosheet. For example, some 2D materials with artificial nanochannels, such as graphene, graphene oxide, and MoS_2,[25,44−47] exhibit favorable membrane seawater desalination performance. Traditionally, in order to obtain a high-performance 2D membrane, additional nanopores must be created artificially with high pore to surface density, and the size of these pores plays a key role in the water transport process.[45] However, current approaches for producing nanopores in 2D membranes confront difficulties since they are frequently complex, lack exact control over pore density and regularity, and cannot be scaled up for vast surface areas.[48,49] In particular, it is still extremely difficult to create vertical holes in films.[49,50] A larger pore size enhances water permeability but typically compromises ion rejection efficiency.[25] As depicted in Figure 2a, several approaches have been utilized to create a 2D membrane with nanopores, such as bombardment by electrons, ions, or with O_2 plasma treatment.[25] Although membranes with pore areas of 40−50 $Å^2$ are predicted to exhibit the best water permeability and satisfactory ion rejection rate,[19,44,51] it is still very challenging to control the size of nanopores experimentally. Uniformly controlling the nanopore size remains difficult, and excessive pore density substantially weakens membrane mechanical integrity.[52,53]

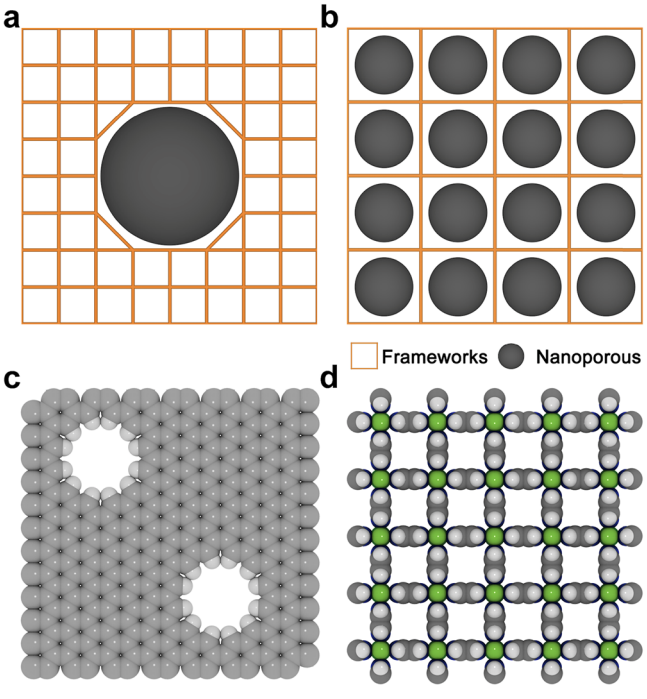

Figure 2. Illustration of two strategies for generating pore architectures in porous materials suitable for water desalination. (a) Traditional 2D membrane with artificial pores created by electron/ion bombardments or with O_2 plasma treatment. (b) Our $NiF_2(pyz)_2$ membrane with intrinsic small pore size structure. (c) Top view of the graphene pore structure (labeled as Gr_2) and (d) $NiF_2(pyz)_2$ MOF structure. Color scheme: C, gray; H, white; Ni, cyan; F, green; N, blue.

The $NiF_2(pyz)_2$ membrane, featuring intrinsically small pore sizes (Figure 2b), is proposed as a promising alternative for achieving outstanding desalination performance. It is worth noting that $NiF_2(pyz)_2$ is an energetically stable freestanding structure with high mechanical strength, enabling it to withstand the pressures required to overcome osmotic pressure during desalination.[27] More importantly, we demonstrate that the $NiF_2(pyz)_2$ structure remains stable in the presence of water,[27] confirming its suitability for desalination applications. This stability suggests that the 2D framework can retain its structural integrity throughout the water transport process.

We further suggest that rather than relying on a single large pore as in conventional 2D membranes, a high pore area-to-surface area ratio is more effective for maximizing water permeability. To assess this feature, we defined a simple constant, φ:

$$\varphi = \frac{\sum_i A_{\text{pore}}}{r_{\text{Largest}}^2}$$

where A_{pore} is the pore area and r_{Largest} represents the largest pore size (in diameter) of the membrane. Therefore, one can expect that the larger the φ value, the higher the permeability of the 2D membrane.

To validate these design principles, in addition to the $NiF_2(pyz)_2$ monolayer (φ = 19.63), we equally constructed two nanoporous graphene models with lower φ values than the 2D MOF and distinct pore density, i.e., **Gr_1** (φ = 0.79) and **Gr_2** (φ = 1.57; see Figure 2c and the Supporting Information for model details).

Figure 3a shows the simulation box of the $NiF_2(pyz)_2$ membrane, along with a plot of the number of filtered water molecules transported through the membrane as a function of MD simulation time under varying applied pressures (Figure 3b). Figure 3c shows that the resulting water flux increases linearly with applied pressure, implying that our findings remain also valid at low pressures (i.e., typical industrial membrane for desalination with a few MPa). The impact of pore density on water permeability performance was further assessed by comparison with the **Gr_1** and **Gr_2** graphene models described above. Under the same pressure condition (150 MPa), the $NiF_2(pyz)_2$ membrane shows an ultrahigh water permeability of 1.37×10^6 L m^{-2} h^{-1}, 1 order of magnitude higher than that of **Gr_1** (3.54×10^5 L m^{-2} h^{-1}). These results highlight that a high water permeability can be obtained when a high pore area-to-surface area ratio is favored. Figure 3d shows that salt rejection is 100% for the $NiF_2(pyz)_2$ membrane under the distinct applied pressure. Notably, under higher applied pressures (>200 MPa), the number of water molecules permeating through the $NiF_2(pyz)_2$ membrane reaches a plateau. This behavior results from the depletion of feedside water molecules before the simulation concludes. Importantly, the membrane maintains a 100% salt rejection rate (*cf.* Figure S1), in stark contrast with the significant decline in salt rejection typically observed under comparable pressures in conventional 2D membranes featuring artificial

https://doi.org/10.1021/acs.chemmater.5c01510
Chem. Mater. 2025, 37, 8627−8635

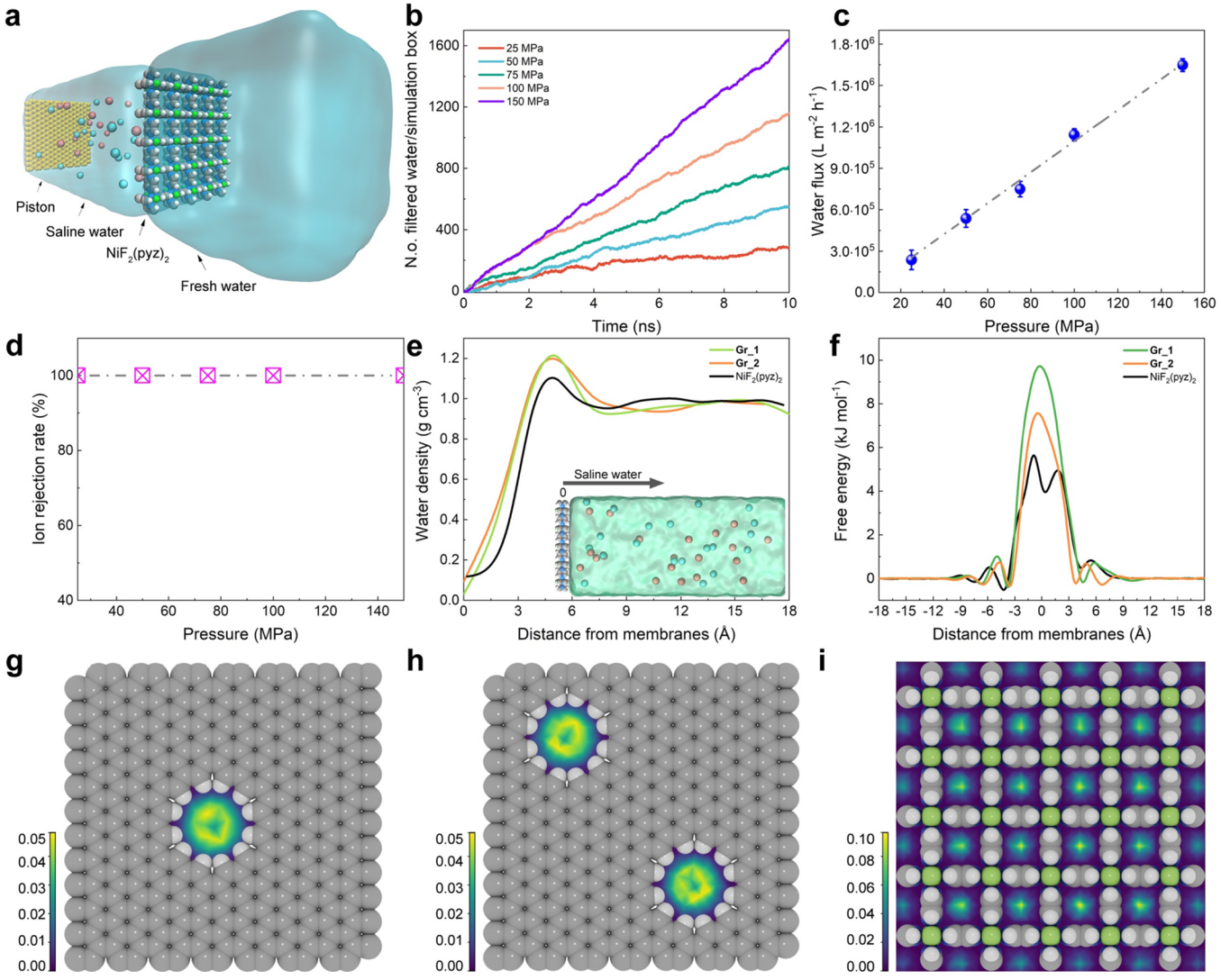

Figure 3. Water permeation and salt rejection through the $NiF_2(pyz)_2$ membrane. (a) Schematic of the membrane simulation box consisting of a piston, saline water with Na^+ and Cl^- ions, [001]-oriented MOF membrane, and freshwater section. (b) Number of water molecules passing through the $NiF_2(pyz)_2$ as a function of the MD simulations at distinct applied pressures of 25, 50, 75, 100, and 150 MPa. (c) Water flux of $NiF_2(pyz)_2$ with respect to applied external pressure. The error bars were extracted from three independent runs. (d) Ion rejection rate of $NiF_2(pyz)_2$ with respect to the applied pressure from 25 to 150 MPa. (e) Simulated water density with respect to the distance from membranes in the saline water part of the simulation boxes (150 MPa). The inset shows the saline section of the simulation box along the *x*-axis, where 0 is the center of the membranes. (f) Calculated potential mean force (PMF) of water molecules for the three different membranes. Calculated 2D density (number of water molecules per Å^3) profiles (along the *x* and *y* directions) of the water molecules located in the pore zone for (g) Gr_1, (h) Gr_2, and (i) $NiF_2(pyz)_2$ monolayer, respectively.

nanopores. For example, the salt rejection rate of the **Gr_2** model decreases when the applied pressure is higher than 200 MPa (*cf.* Figures S3 and S4) and many other studies.[54] The excellent water desalination performance of $NiF_2(pyz)_2$ makes this membrane a promising material for energy-efficient desalination technology.

To gain deeper insight into the exceptional performance of $NiF_2(pyz)_2$, we calculated the density of water near the membrane surface on the saline side (Figure 3e). $NiF_2(pyz)_2$ exhibits a lower water density peak near its surface compared to the **Gr_1** and **Gr_2** models. This facilitates water penetration through the MOF channel, as the static pressure is proportional to water density. We also computed the potential of mean force (PMF) for a water molecule passing through the membranes. To ensure an unbiased computation of the PMF, we carried out equilibrium simulations with zero applied pressure for a duration of 10 ns. The PMF was determined using the equation $\text{PMF} = -K_B T \ln\left[\frac{\rho(z)}{\rho_0}\right]$, where $\rho(z)$ is the density of water at z and ρ_0 is the equilibrium density of water. Figure 3f reports the corresponding PMF of water for each membrane within a distance of 20 Å from both sides. Compared to the **Gr_1** and **Gr_2** membranes, the $NiF_2(pyz)_2$ monolayer shows a lower potential of mean force (PMF) peaks, reflecting reduced energy barriers for water transport and consequently promoting more efficient water permeation through its confined nanochannels. Moreover, while the $NiF_2(pyz)_2$ monolayer has a larger number of pores per unit area (φ values: 0.79, 1.57, and 19.63 for **Gr_1**, **Gr_2**, and $NiF_2(pyz)_2$, respectively), it has also a slightly higher water density near the pores as shown in Figure 3g–i, resulting in a more rapid H_2O permeation in this membrane.

https://doi.org/10.1021/acs.chemmater.5c01510
Chem. Mater. 2025, 37, 8627−8635

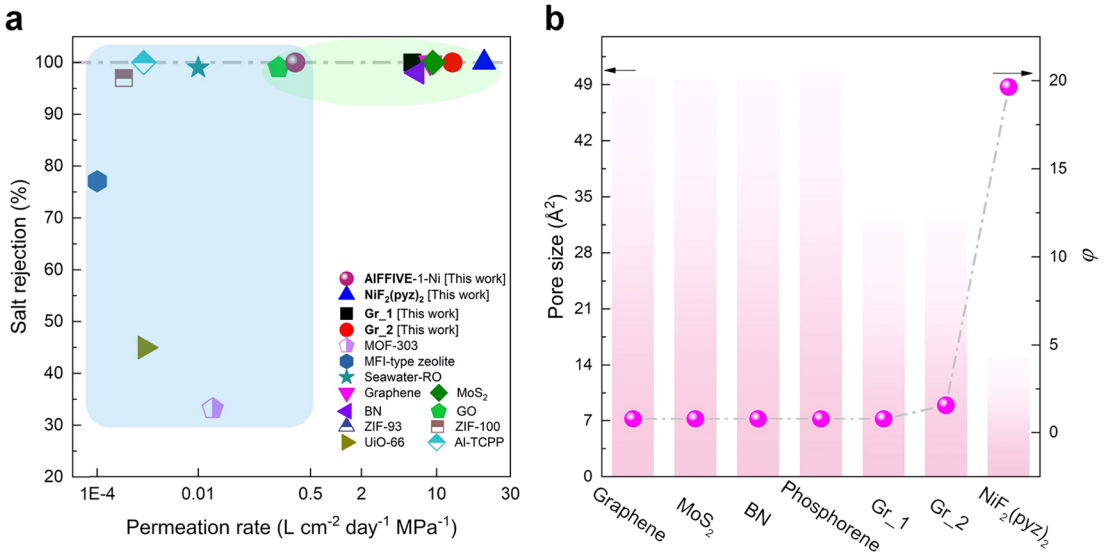

Figure 4. Desalination performance of the $NiF_2(pyz)_2$ membrane vs other membranes. (a) Water permeability and ion rejection rate of the different explored membranes in this work and others reported in the literature.[18,23,44,51,56] For a fair comparison, we represent the porous membranes and the 2D material in different color regions. Water permeability with the same unit (L cm^{-2} day^{-1} MPa^{-1}) was used for the standard comparison. (b) Calculated φ and pore size (Å^2) of graphene, MoS_2, BN, phosphorene, **Gr_1**, **Gr_2**, and $NiF_2(pyz)_2$ membranes. For graphene, MoS_2, BN, and phosphorene, the models from ref 51 were used to calculate φ.

To estimate the activation energy of water permeation in the membranes, water flux was calculated at 150 MPa across a temperature range of 280 to 310 K in 10 K increments (*cf.* Figure S5). Given that the **Gr_2** model is more artificial, as the distance between adjacent pores can significantly influence the water permeation, we focused the comparative analysis between $NiF_2(pyz)_2$ and **Gr_1** membranes. By fitting the data to the Arrhenius equation, the activation energy for water transport through the $NiF_2(pyz)_2$ membrane was determined to be 15.8 kJ mol^{-1}, which is lower than the value calculated for **Gr_1** (19.3 kJ mol^{-1}) and ZIF-8 (24.4 kJ mol^{-1})[55] membranes. This reduced energy barrier, in combination with a higher water density near the pores and the larger φ value, contributes to the ultrafast water flux observed in the $NiF_2(pyz)_2$ monolayer.

Overall, our simulation results highlight that the $NiF_2(pyz)_2$ membrane is a highly promising candidate for desalination, offering high water permeability and maintaining 100% salt rejection across all applied pressure ranges as summarized in Figure 4a. Notably, the $NiF_2(pyz)_2$ membrane enables an excellent water permeation, more than 4 orders of magnitude higher than UiO-66(Zr) (cage-based MOF) and the 2D Al-TCPP (1D channel-based MOF).[18,23] Therefore, the high water permeability of the $NiF_2(pyz)_2$ membrane can be understood in light of the value of the descriptors introduced in this work,φ, which is related to the pore area-to-surface area ratio. Figure 4b emphasizes that although the already proposed 2D membranes with artificial nanopores, such as graphene, MoS_2, *etc.*, have a large pore size (~50 Å^2), compared with the $NiF_2(pyz)_2$ membrane (14.9 Å^2), the calculated φ of all these membranes are much lower (~0.78) compared with that of the $NiF_2(pyz)_2$ membrane (~19.64), resulting in a significant obstacle to water permeability. For membranes with artificial nanopores, water permeability can be improved by increasing its pore size (>50 Å^2); however, this typically results in a significant reduction in ion rejection efficiency. Meanwhile, traditional 2D membranes, such as porous graphene, rely on artificial pore fabrication, which inevitably results in nonuniform pore sizes.[25,57] This intrinsic structural irregularity underpins the permeability-selectivity trade-off. Specifically, even a minor increase of pore size due to defect formation enables ion leakage while attempts to boost flux by increasing pore density or diameter compromise mechanical robustness of the membrane. In sharp contrast, the $NiF_2(pyz)_2$ monolayer offers an intrinsically ordered architecture, where atomically precise pores provide excellent structural uniformity. This design ensures ultrahigh water permeability combined with 100% ion rejection, thus reconciling the trade-off between permeability and selectivity. Therefore, our proposed $NiF_2(pyz)_2$ membrane shows optimal performance for water desalination combining efficiency, selectivity, and mechanical stability.

CONCLUSIONS

In this work, we introduce a potential design strategy for high-performance desalination membranes grounded in the use of structurally precise, intrinsically porous MOFs. Through molecular dynamics simulations, the 2D $NiF_2(pyz)_2$ monolayer, a mechanically and hydrothermally stable MOF with well-aligned ultrasmall channels with a pore size of ~4 Å, is predicted to exhibit exceptional water transport permeability while maintaining 100% Na^+/Cl^- rejection across a wide range of operating pressures, including extreme values exceeding 200 MPa. Our study reveals that the remarkable performance of this membrane stems from a synergistic combination of favorable water density distribution at the interface, low free energy barriers for water diffusion, and a uniquely high pore area-to-surface area ratio, captured by a dimensionless descriptor φ. This molecular-level understanding is further supported by comparative analysis with conventional 2D membranes such as graphene and MoS_2, where artificial nanopores often suffer from fabrication complexity, limited scalability, and a permeability-selectivity trade-off. By defying the long-standing paradigm that favors large, inhomogeneous nanopores to enhance water flux, the $NiF_2(pyz)_2$ monolayer establishes a promising framework for membrane design: one

https://doi.org/10.1021/acs.chemmater.5c01510
Chem. Mater. 2025, 37, 8627−8635

that leverages intrinsically uniform, angstrom-scale porosity to reconcile ultrafast water transport with complete salt rejection. It is worth noting that, although the perfect $NiF_2(pyz)_2$ monolayer was designed using computational approaches, its synthesizability is supported by experimental realization of a stable analogous monolayer compound, i.e., $NiCl_2(pyz)_2$, etc., as well as layered $NiF_2(pyz)_2$ structures.[58−60] This work not only advances the fundamental understanding of water transport in nanoporous systems but also paves the way toward scalable, energy-efficient, and next-generation desalination technologies based on MOF monolayers.

■ ASSOCIATED CONTENT

Supporting Information

The Supporting Information is available free of charge at https://pubs.acs.org/doi/10.1021/acs.chemmater.5c01510.

Detailed data of the simulation models, force field parameters, water fluxes, and Na^+/Cl^- rejection rates at different pressure for the **Gr_1** and **Gr_2** models, an Arrhenius plot of water flux for $NiF_2(pyz)_2$ and the **Gr_1** nanopore graphene membrane (PDF)

Video of the process of seawater desalination using the **AlFFIVE**-1-Ni MOF model (MP4)

Video of the process of seawater desalination using the $NiF_2(pyz)_2$ model (MOV)

■ AUTHOR INFORMATION

Corresponding Author

Guillaume Maurin − *ICGM, Université de Montpellier, CNRS, ENSCM, Montpellier 34293, France; Institut Universitaire de France (IUF), Paris, France;* orcid.org/0000-0002-2096-0450; Email: guillaume.maurin1@umontpellier.fr

Authors

Dong Fan − *School of Materials Science and Engineering, Chongqing Jiaotong University, Chongqing 400074, China; ICGM, Université de Montpellier, CNRS, ENSCM, Montpellier 34293, France;* orcid.org/0000-0003-1873-3416

Ke Zheng − *School of Materials Science and Engineering, Chongqing Jiaotong University, Chongqing 400074, China;* orcid.org/0009-0005-3559-1319

Supriyo Naskar − *ICGM, Université de Montpellier, CNRS, ENSCM, Montpellier 34293, France;* orcid.org/0000-0002-3690-6483

Complete contact information is available at: https://pubs.acs.org/10.1021/acs.chemmater.5c01510

Author Contributions

D.F. and G.M. designed the research. D.F., K.Z., and S.N. carried out the simulations. All authors wrote the manuscript. G.M. supervised the research.

Notes

The authors declare no competing financial interest.

■ ACKNOWLEDGMENTS

The computational work was performed using HPC resources from GENCI-CINES (Grant A0180907613). This work was also supported by the Science and Technology Research Program of Chongqing Municipal Education Commission (Grant No. KJQN202500748). G.M. thanks Institut Universitaire de France for the Senior Chair.

■ REFERENCES

(1) Larsen, T. A.; Hoffmann, S.; Lüthi, C.; Truffer, B.; Maurer, M. Emerging Solutions to the Water Challenges of an Urbanizing World. *Science* **2016**, *352* (6288), 928−933.

(2) Abbott, B. W.; Bishop, K.; Zarnetske, J. P.; Minaudo, C.; Chapin, F. S.; Krause, S.; Hannah, D. M.; Conner, L.; Ellison, D.; Godsey, S. E.; Plont, S.; Marçais, J.; Kolbe, T.; Huebner, A.; Frei, R. J.; Hampton, T.; Gu, S.; Buhman, M.; Sara Sayedi, S.; Ursache, O.; Chapin, M.; Henderson, K. D.; Pinay, G. Human Domination of the Global Water Cycle Absent from Depictions and Perceptions. *Nat. Geosci.* **2019**, *12* (7), 533−540.

(3) Scanlon, B. R.; Fakhreddine, S.; Rateb, A.; de Graaf, I.; Famiglietti, J.; Gleeson, T.; Grafton, R. Q.; Jobbagy, E.; Kebede, S.; Kolusu, S. R.; Konikow, L. F.; Long, D.; Mekonnen, M.; Schmied, H. M.; Mukherjee, A.; MacDonald, A.; Reedy, R. C.; Shamsudduha, M.; Simmons, C. T.; Sun, A.; Taylor, R. G.; Villholth, K. G.; Vörösmarty, C. J.; Zheng, C. Global Water Resources and the Role of Groundwater in a Resilient Water Future. *Nat. Rev. Earth Environ* **2023**, *4* (2), 87−101.

(4) Elimelech, M.; Phillip, W. A. The Future of Seawater Desalination: Energy, Technology, and the Environment. *Science* **2011**, *333* (6043), 712−717.

(5) Yao, Y.; Zhang, P.; Jiang, C.; DuChanois, R. M.; Zhang, X.; Elimelech, M. High Performance Polyester Reverse Osmosis Desalination Membrane with Chlorine Resistance. *Nat. Sustain* **2021**, *4* (2), 138−146.

(6) Shen, J.; Cai, Y.; Zhang, C.; Wei, W.; Chen, C.; Liu, L.; Yang, K.; Ma, Y.; Wang, Y.; Tseng, C.-C.; Fu, J.-H.; Dong, X.; Li, J.; Zhang, X.-X.; Li, L.-J.; Jiang, J.; Pinnau, I.; Tung, V.; Han, Y. Fast Water Transport and Molecular Sieving through Ultrathin Ordered Conjugated-Polymer-Framework Membranes. *Nat. Mater.* **2022**, *21* (10), 1183−1190.

(7) Zhang, Q.; Gao, B.; Zhang, L.; Liu, X.; Cui, J.; Cao, Y.; Zeng, H.; Xu, Q.; Cui, X.; Jiang, L. Anomalous Water Molecular Gating from Atomic-Scale Graphene Capillaries for Precise and Ultrafast Molecular Sieving. *Nat. Commun.* **2023**, *14* (1), 6615.

(8) Furukawa, H.; Cordova, K. E.; O'Keeffe, M.; Yaghi, O. M. The Chemistry and Applications of Metal-Organic Frameworks. *Science* **2013**, *341* (6149), No. 1230444.

(9) Wang, H.; Fang, T.; Wang, J.; Zhang, M.; Mu, X.; Gao, T.; Wei, T.; Dai, Z. Adaptive Size Evolution of an MOFs-in-MOF Nanovehicle for Enhanced Nucleus-Targeted Tumor Chemotherapy. *Nano Lett.* **2024**, *24* (34), 10605−10613.

(10) Le Huec, T.; López-Francés, A.; Abánades Lázaro, I.; Navalón, S.; Baldoví, H. G.; Giménez-Marqués, M. Heteroepitaxial MOF-on-MOF Photocatalyst for Solar-Driven Water Splitting. *ACS Nano* **2024**, *18* (31), 20201−20212.

(11) Park, C.; Shin, H.; Jeon, M.; Cho, S. H.; Kim, J.; Kim, I. D. Single-Atom Catalysts in Conductive Metal-Organic Frameworks: Enabling Reversible Gas Sensing at Room Temperature. *ACS Nano* **2024**, No. acsnano.4c05815.

(12) Wang, C.; Liu, X.; Keser Demir, N.; Chen, J. P.; Li, K. Applications of Water Stable Metal-Organic Frameworks. *Chem. Soc. Rev.* **2016**, *45* (18), 5107−5134.

(13) Ji, Z.; Wang, H.; Canossa, S.; Wuttke, S.; Yaghi, O. M. Pore Chemistry of Metal-Organic Frameworks. *Adv. Funct. Mater.* **2020**, *30* (41), No. 2000238.

(14) Jiang, H.; Alezi, D.; Eddaoudi, M. A Reticular Chemistry Guide for the Design of Periodic Solids. *Nat. Rev. Mater.* **2021**, *6* (6), 466−487.

(15) Cheng, Y.; Datta, S. J.; Zhou, S.; Jia, J.; Shekhah, O.; Eddaoudi, M. Advances in Metal-Organic Framework-Based Membranes. *Chem. Soc. Rev.* **2022**, *51* (19), 8300−8350.

(16) Zhou, S.; Shekhah, O.; Ramírez, A.; Lyu, P.; Abou-Hamad, E.; Jia, J.; Li, J.; Bhatt, P. M.; Huang, Z.; Jiang, H.; Jin, T.; Maurin, G.; Gascon, J.; Eddaoudi, M. Asymmetric Pore Windows in MOF

Membranes for Natural Gas Valorization. *Nature* **2022**, *606* (7915), 706−712.
(17) Datta, S. J.; Mayoral, A.; Murthy Srivatsa Bettahalli, N.; Bhatt, P. M.; Karunakaran, M.; Carja, I. D.; Fan, D.; Graziane M. Mileo, P.; Semino, R.; Maurin, G.; Terasaki, O.; Eddaoudi, M. Rational Design of Mixed-Matrix Metal-Organic Framework Membranes for Molecular Separations. *Science* **2022**, *376* (6597), 1080−1087.
(18) Liu, X.; Demir, N. K.; Wu, Z.; Li, K. Highly Water-Stable Zirconium Metal-Organic Framework UiO-66 Membranes Supported on Alumina Hollow Fibers for Desalination. *J. Am. Chem. Soc.* **2015**, *137* (22), 6999−7002.
(19) Cao, Z.; Liu, V.; Barati Farimani, A. Water Desalination with Two-Dimensional Metal-Organic Framework Membranes. *Nano Lett.* **2019**, *19* (12), 8638−8643.
(20) Liu, Y. C.; Yeh, L. H.; Zheng, M. J.; Wu, K. C. W. Highly Selective and High-Performance Osmotic Power Generators in Subnanochannel Membranes Enabled by Metal-Organic Frameworks. *Sci. Adv.* **2021**, *7* (10), No. eabe9924.
(21) Cong, S.; Yuan, Y.; Wang, J.; Wang, Z.; Kapteijn, F.; Liu, X. Highly Water-Permeable Metal-Organic Framework MOF-303 Membranes for Desalination. *J. Am. Chem. Soc.* **2021**, *143* (48), 20055−20058.
(22) Zhang, H.; Hou, J.; Hu, Y.; Wang, P.; Ou, R.; Jiang, L.; Liu, J. Z.; Freeman, B. D.; Hill, A. J.; Wang, H. Ultrafast Selective Transport of Alkali Metal Ions in Metal Organic Frameworks with Subnanometer Pores. *Sci. Adv.* **2018**, *4* (2), No. eaaq0066.
(23) Jian, M.; Qiu, R.; Xia, Y.; Lu, J.; Chen, Y.; Gu, Q.; Liu, R.; Hu, C.; Qu, J.; Wang, H.; Zhang, X. Ultrathin Water-Stable Metal-Organic Framework Membranes for Ion Separation. *Sci. Adv.* **2020**, *6* (23), No. eaay3998.
(24) Werber, J. R.; Osuji, C. O.; Elimelech, M. Materials for Next-Generation Desalination and Water Purification Membranes. *Nat. Rev. Mater.* **2016**, *1* (5), 16018.
(25) Surwade, S. P.; Smirnov, S. N.; Vlassiouk, I. V.; Unocic, R. R.; Veith, G. M.; Dai, S.; Mahurin, S. M. Water Desalination Using Nanoporous Single-Layer Graphene. *Nat. Nanotechnol.* **2015**, *10* (5), 459−464.
(26) Abraham, J.; Vasu, K. S.; Williams, C. D.; Gopinadhan, K.; Su, Y.; Cherian, C. T.; Dix, J.; Prestat, E.; Haigh, S. J.; Grigorieva, I. V.; Carbone, P.; Geim, A. K.; Nair, R. R. Tunable Sieving of Ions Using Graphene Oxide Membranes. *Nat. Nanotechnol.* **2017**, *12* (6), 546−550.
(27) Fan, D.; Ozcan, A.; Lyu, P.; Maurin, G. Unravelling Abnormal In-Plane Stretchability of Two-Dimensional Metal-Organic Frameworks by Machine Learning Potential Molecular Dynamics. *Nanoscale* **2024**, *16* (7), 3438−3447.
(28) Li, J.-R.; Kuppler, R. J.; Zhou, H.-C. Selective Gas Adsorption and Separation in Metal-Organic Frameworks. *Chem. Soc. Rev.* **2009**, *38* (5), 1477.
(29) Itoh, Y.; Chen, S.; Hirahara, R.; Konda, T.; Aoki, T.; Ueda, T.; Shimada, I.; Cannon, J. J.; Shao, C.; Shiomi, J.; Tabata, K. V.; Noji, H.; Sato, K.; Aida, T. Ultrafast Water Permeation through Nanochannels with a Densely Fluorous Interior Surface. *Science* **2022**, *376* (6594), 738−743.
(30) Belmabkhout, Y.; Bhatt, P. M.; Adil, K.; Pillai, R. S.; Cadiau, A.; Shkurenko, A.; Maurin, G.; Liu, G.; Koros, W. J.; Eddaoudi, M. Natural Gas Upgrading Using a Fluorinated MOF with Tuned H2S and CO2 Adsorption Selectivity. *Nat. Energy* **2018**, *3* (12), 1059−1066.
(31) Thompson, A. P.; Aktulga, H. M.; Berger, R.; Bolintineanu, D. S.; Brown, W. M.; Crozier, P. S.; in 't Veld, P. J.; Kohlmeyer, A.; Moore, S. G.; Nguyen, T. D.; Shan, R.; Stevens, M. J.; Tranchida, J.; Trott, C.; Plimpton, S. J. LAMMPS - a Flexible Simulation Tool for Particle-Based Materials Modeling at the Atomic, Meso, and Continuum Scales. *Comput. Phys. Commun.* **2022**, *271*, No. 108171.
(32) Humphrey, W.; Dalke, A.; Schulten, K. VMD: Visual Molecular Dynamics. *J. Mol. Graphics* **1996**, *14* (1), 33−38.
(33) Abascal, J. L. F.; Vega, C. A General Purpose Model for the Condensed Phases of Water: TIP4P/2005. *J. Chem. Phys.* **2005**, *123* (23), No. 234505.
(34) Ryckaert, J.-P.; Ciccotti, G.; Berendsen, H. J. C. Numerical Integration of the Cartesian Equations of Motion of a System with Constraints: Molecular Dynamics of n-Alkanes. *J. Comput. Phys.* **1977**, *23* (3), 327−341.
(35) Berendsen, H. J. C.; Grigera, J. R.; Straatsma, T. P. The Missing Term in Effective Pair Potentials. *J. Phys. Chem.* **1987**, *91* (24), 6269−6271.
(36) Horn, H. W.; Swope, W. C.; Pitera, J. W.; Madura, J. D.; Dick, T. J.; Hura, G. L.; Head-Gordon, T. Development of an Improved Four-Site Water Model for Biomolecular Simulations: TIP4P-Ew. *J. Chem. Phys.* **2004**, *120* (20), 9665−9678.
(37) Lorentz, H. A. Ueber Die Anwendung Des Satzes Vom Virial in Der Kinetischen Theorie Der Gase. *Annalen der physik* **1881**, *248* (1), 127−136.
(38) Essmann, U.; Perera, L.; Berkowitz, M. L.; Darden, T.; Lee, H.; Pedersen, L. G. A Smooth Particle Mesh Ewald Method. *J. Chem. Phys.* **1995**, *103* (19), 8577−8593.
(39) Nosé, S. A Unified Formulation of the Constant Temperature Molecular Dynamics Methods. *J. Chem. Phys.* **1984**, *81* (1), 511−519.
(40) Hoover, W. G. Canonical Dynamics: Equilibrium Phase-Space Distributions. *Phys. Rev. A* **1985**, *31* (3), 1695−1697.
(41) Rappe, A. K.; Casewit, C. J.; Colwell, K. S.; Goddard, W. A.; Skiff, W. M. UFF, a Full Periodic Table Force Field for Molecular Mechanics and Molecular Dynamics Simulations. *J. Am. Chem. Soc.* **1992**, *114* (25), 10024−10035.
(42) Manz, T. A.; Limas, N. G. Introducing DDEC6 Atomic Population Analysis: Part 1. Charge Partitioning Theory and Methodology. *RSC Adv.* **2016**, *6* (53), 47771−47801.
(43) Lyu, Q.; Deng, X.; Hu, S.; Lin, L.-C.; Ho, W. S. W. Exploring the Potential of Defective UiO-66 as Reverse Osmosis Membranes for Desalination. *J. Phys. Chem. C* **2019**, *123* (26), 16118−16126.
(44) Heiranian, M.; Farimani, A. B.; Aluru, N. R. Water Desalination with a Single-Layer MoS2 Nanopore. *Nat. Commun.* **2015**, *6* (1), 8616.
(45) Homaeigohar, S.; Elbahri, M. Graphene Membranes for Water Desalination. *NPG Asia Mater.* **2017**, *9* (8), e427−e427.
(46) Morelos-Gomez, A.; Cruz-Silva, R.; Muramatsu, H.; Ortiz-Medina, J.; Araki, T.; Fukuyo, T.; Tejima, S.; Takeuchi, K.; Hayashi, T.; Terrones, M.; Endo, M. Effective NaCl and Dye Rejection of Hybrid Graphene Oxide/Graphene Layered Membranes. *Nat. Nanotechnol.* **2017**, *12* (11), 1083−1088.
(47) Wang, W.; Onofrio, N.; Petit, E.; Karamoko, B. A.; Wu, H.; Liu, J.; Li, J.; Qi, K.; Zhang, Y.; Gervais, C.; Lajaunie, L.; Salameh, C.; Miele, P.; Zeng, Z.; Voiry, D. High-Surface-Area Functionalized Nanolaminated Membranes for Energy-Efficient Nanofiltration and Desalination in Forward Osmosis. *Nat. Water* **2023**, *1* (2), 187−197.
(48) Han, T. H.; Huang, Y.-K.; Tan, A. T. L.; Dravid, V. P.; Huang, J. Steam Etched Porous Graphene Oxide Network for Chemical Sensing. *J. Am. Chem. Soc.* **2011**, *133* (39), 15264−15267.
(49) Olejniczak, A.; Rymzhanov, R. A. From Nanohole to Ultralong Straight Nanochannel Fabrication in Graphene Oxide with Swift Heavy Ions. *Nat. Commun.* **2023**, *14* (1), 889.
(50) Liu, M.; Weston, P. J.; Hurt, R. H. Controlling Nanochannel Orientation and Dimensions in Graphene-Based Nanofluidic Membranes. *Nat. Commun.* **2021**, *12* (1), 507.
(51) Cao, Z.; Liu, V.; Barati Farimani, A. Why Is Single-Layer MoS 2 a More Energy Efficient Membrane for Water Desalination? *ACS Energy Lett.* **2020**, *5* (7), 2217−2222.
(52) Cohen-Tanugi, D.; Grossman, J. C. Mechanical Strength of Nanoporous Graphene as a Desalination Membrane. *Nano Lett.* **2014**, *14* (11), 6171−6178.
(53) Mi, B. Scaling up Nanoporous Graphene Membranes. *Science* **2019**, *364* (6445), 1033−1034.
(54) Cohen-Tanugi, D.; Grossman, J. C. Water Desalination across Nanoporous Graphene. *Nano Lett.* **2012**, *12* (7), 3602−3608.

https://doi.org/10.1021/acs.chemmater.5c01510
Chem. Mater. 2025, 37, 8627−8635

(55) Hu, Z.; Chen, Y.; Jiang, J. Zeolitic Imidazolate Framework-8 as a Reverse Osmosis Membrane for Water Desalination: Insight from Molecular Simulation. *J. Chem. Phys.* **2011**, *134* (13), 134705.
(56) Gupta, K. M.; Zhang, K.; Jiang, J. Water Desalination through Zeolitic Imidazolate Framework Membranes: Significant Role of Functional Groups. *Langmuir* **2015**, *31* (48), 13230−13237.
(57) Wang, Z.; Ma, C.; Xu, C.; Sinquefield, S. A.; Shofner, M. L.; Nair, S. Graphene oxide nanofiltration membranes for desalination under realistic conditions. *Nat. Sustain* **2021**, *4* (5), 402−408.
(58) Perlepe, P.; Oyarzabal, I.; Mailman, A.; Yquel, M.; Platunov, M.; Dovgaliuk, I.; Rouzières, M.; Négrier, P.; Mondieig, D.; Suturina, E. A.; Dourges, M.-A.; Bonhommeau, S.; Musgrave, R. A.; Pedersen, K. S.; Chernyshov, D.; Wilhelm, F.; Rogalev, A.; Mathonière, C.; Clérac, R. Metal-Organic Magnets with Large Coercivity and Ordering Temperatures up to 242°C. *Science* **2020**, *370* (6516), 587−592.
(59) Pedersen, K. S.; Perlepe, P.; Aubrey, M. L.; Woodruff, D. N.; Reyes-Lillo, S. E.; Reinholdt, A.; Voigt, L.; Li, Z.; Borup, K.; Rouzières, M.; Samohvalov, D.; Wilhelm, F.; Rogalev, A.; Neaton, J. B.; Long, J. R.; Clérac, R. Formation of the Layered Conductive Magnet CrCl2(Pyrazine)2 through Redox-Active Coordination Chemistry. *Nature Chem.* **2018**, *10* (10), 1056−1061.
(60) Manson, J. L.; Manson, Z. E.; Sargent, A.; Villa, D. Y.; Etten, N. L.; Blackmore, W. J. A.; Curley, S. P. M.; Williams, R. C.; Brambleby, J.; Goddard, P. A.; Ozarowski, A.; Wilson, M. N.; Huddart, B. M.; Lancaster, T.; Johnson, R. D.; Blundell, S. J.; Bendix, J.; Wheeler, K. A.; Lapidus, S. H.; Xiao, F.; Birnbaum, S.; Singleton, J. Enhancing Easy-Plane Anisotropy in Bespoke Ni(II) Quantum Magnets. *Polyhedron* **2020**, *180*, No. 114379.

https://doi.org/10.1021/acs.chemmater.5c01510
Chem. Mater. 2025, 37, 8627−8635